Mathematical Analysis of Hall Effect and Hematocrit Dependent Viscosity on Au/GO-Blood Hybrid Nanofluid Flow Through a Stenosed Catheterized Artery with Thrombosis

Umesh Khanduri(✉) and B. K. Sharma

Department of Mathematics, Birla Institute of Technology and Science Pilani, Pilani, Rajasthan, India
umeshkhanduri09@gmail.com

Abstract. The present paper addresses the rheological perspective of blood flow with the suspension of Au/GO nanoparticles through the curved artery with multiple stenosis and thrombosis. The influences of hematocrit-dependent viscosity and Hall effects are taken into account. The flow is subjected to a strong radial magnetic field. Using the mild stenosis and axi-directional flow assumptions, the governing equations are simplified and then the reduced equations are discretize using the Crank-Nicholson technique to get the tridiagonal systems of equations which are further solved by employing the Tri-diagonal Matrix Algorithm (TDMA) at each time step. The flow patterns are also shown by plotting velocity contours. It has been observed that raising the Hall parameter induces an increase in fluid velocity owing to an increase in collision time or electron frequency, hence assisting fluid flow. Further, Au-GO/blood hybrid nanoparticles have a higher velocity profile than pure blood and unitary nanoparticles. Current findings may have applications in the biomedical field, particularly in imaging techniques like magnetic resonance angiography (MRA), which analyses an image of an artery to detect problems. The current findings are consistent with recent findings in earlier blood flow research studies.

Keywords: Stenosis · Hybrid nanoparticles · Hall effect · Clot

1 Introduction

Among the various cardiovascular diseases, arteriosclerosis/stenosis is the major cause of morbidity and mortality worldwide [1]. Arteriosclerosis is a condition in which plaque gets deposited at the arterial wall and constricts the blood flow. The plaque is the composition of fats/lipids, cholesterol, greasy substances, and other cellular wastes. The constriction may trigger thrombosis (blood clot) upon rupture and lead to a heart attack. Doffin et al. [2] experimented with

J. Singh et al. (Eds.): ICMMAAC 2022, LNNS 666, pp. 121–137, 2023.
https://doi.org/10.1007/978-3-031-29959-9_8

studying the oscillatory flow between the clot and stenosis model. The oscillation is produced by the two pistons moving in the oscillate phase. They determined the velocity and streamlined pattern by visualising the suspended aluminium particles in water glycerol fluid. Strony et al. [3] investigated the high shear stress effect and hemodynamic factors for the thrombus deposition in the stenotic region. According to their study, the shear stress would be higher in the stenotic region, which causes the platelets to get aggregated at the vessel wall damage and from the occlusive thrombosis. Elnaqeeb et al. [4] explored the copper blood model due to its application in biomedicine. They also discovered the blood tapering phenomenon in catheterised stenosis arteries. The time-variant stenosis with an aneurysm was numerically explored by Sultan et al. [5]. They considered the non-Newtonian Eyring Powell fluid model and curvilinear coordinate system to study the blood flow through the curved artery. Akthar et al. [6] developed a mathematical model to simulate the blood flow through multiple thromboses with the Peristaltic wall.

In the magnetic field, moving conducting fluids experience a resistive force known as Lorentz force. When the moving fluid is ionised gas, or the strong magnetic field is applied, the conductivity normal to the magnetic field is reduced. This reduction is due to the free spinning of the electrons. Thus, it induces the electric current normal to the magnetic and electric field. This phenomenon is known as Hall current. Mekheimer et al. [7] studied the Hall effect with viscous dissipation on the micropolar fluid through the stenosis artery. Mishra et al. [8] experimented to understand the Hall and magnetic field effect on the MHD flow through the rotating channel. Das et al. [9] conducted theoretical research to investigate peristaltic blood pumping. They examined the Hall and ion slip effects by using Casson fluid to mimic the rheological properties of blood.

Nanotechnology advancements and designing techniques help researchers probe into the nanoscale particles' properties and features. In the biomedical field, the advancement of nanotechnology helps design nanomedicine to diagnose and treat diseases. Nanoparticles are small tiny particles, and with the suspension in the base fluid, they enhance the characteristics and properties of the base fluid. In this study, we have considered the hybrid nanofluid by the suspension of Graphene Oxide and Gold nanoparticles in the base fluid (blood). Elnaqeeb et al. [10] studied the gold nanoparticle's blood flow through the tapered artery and did a comparative study for gold, Cu, and TiO2 nanoparticles. They looked at temperature-dependent viscosity and observed that the velocity of gold nanoparticles in a stenosed blood artery is greater than the other two nanoparticles. Thus, explaining the enhancement in the hemodynamic performance of blood in the diseased artery. Changdar et al. developed a single and discrete phase model to observe the effect of gold, Cu, and silver nanoparticles as drug carriers. They have considered multiple stenoses and spherical-shaped nanoparticles. According to their findings, cylindrical nanoparticles are more effective than spherical nanoparticles in drug delivery. Mekheimer et al. [11] examined the gold nanoparticles in the peristaltic flow between the two coaxial tubes. They contemplated the gold nanoparticles due to their application in treating cancerous cells. Seo Kyung et al. [12] formed the hybrid sheet of Au-GO nanoparticles to enhance the photothermic

effect helpful in cancer therapy. Further, Liu et al. [13] studied graphene-based nanoparticles in their work. They considered graphene nanoparticles due to their photothermal effect beneficial in cancer treatment. Khazayinejad et al. [14] analytically solved the mathematical model portraying graphene nanoparticles' suspension in a tube with wavy walls. Through the use of particle shape factor, slip, and convective regime, Sindhu et al. [15] analysed the flow of a hybrid nanoliquid in a microchannel. Rishu et al. [16] considered the bell-shaped artery with temperature-dependent viscosity to explore the effect of hybrid nanoparticles (Au-Al_2O_3) on blood flow. Furthermore, they [17] investigated the entropy analysis of the MHD slip flow with tapered multiple-stenosis artery.

Blood flow is greatly influenced by pressure, viscosity, and other external and internal elements in the human circulatory system. Blood's hemodynamic properties are constantly changing due to its shear-thinning feature. As a result, blood viscosity cannot be assumed to be constant. Singh et al. [18] explored the Jeffery-Hamel flow in the non-parallel walls by adopting the hybrid computational approach. By employing a hybrid analytical approach, Sushila et al. [19] examined the thin film flow issue. Bhavya et al. [20] studied the inclination and hematocrit dependent viscosity effect on the MHD blood flow. Further, Chandan et al. [21] developed the model by considering the two phase blood flow. Their findings show that radial curvature increases the risk of atherosclerosis whereas heat radiation decreases it. Khanduri and Sharma [22] investigated the entropy generation on the MHD flow by considering the variable viscosity and thermal conductivity. Several other researchers [23–29] developed a mathematical model to illustrate the effect of variable viscosity on MHD flow.

From a bioengineering perspective, it is crucial to research the behaviour of hybrid nanoparticles (Au-GO) suspended by streaming blood flow on the curved stenosed artery in the presence of a strong radial magnetic field; however, no such study has yet been published. The multiple stenosis and thrombosis at the catheter walls hinder the hemodynamic flow. The curvilinear coordinate is customised to simulate blood flow. The current study may be beneficial in radiological examinations such as magnetic resonance angiography (MRA) to detect vascular abnormalities. The hybrid nanoparticles Au-GO/blood have been studied due to their potential applicability in nanomedicine and biomedicine. The inert nature, stability, and anti-bacterial capabilities makes the Au nanoparticles to have the wide range of applications. As a result, the current study sheds light on the treatment of stenosis and other anomalies without surgery while also reducing post-surgical problems. In the future work, the researchers can explored the effect of nanoparticle shapes with the permeable arterial walls along with the different shapes of stenosis (example, triangular and elliptical shapes) with tapering effects can be explored.

The novelty of the present work includes:

- The influence of (Au-GO/blood) hybrid nanoparticles on diseased segments characterized by multiple stenosis and thrombosis.
- To analyze the hematocrit-dependent viscosity model with the combined effect of Hall and body acceleration in the porous medium.

2 Mathematical Formulation

Considered the unsteady, laminar, incompressible, two-dimensional blood flow with suspension of Au/GO nanoparticles through the two coaxial tube forming the constriction due to the thromosis and stenosis. The blood flow is assumed to be Newtonian and axisymmetric. The (r_1, θ_1, z_1) curvilinear coordinate is chosen to mimic the blood flow through a diseased artery. The r and z represent the radial and axial direction respectively. Figure 1 represent the pictorial representation of diseased artery in which the outer tube has the multiple stenosis with radius η and the inner tube has the clot on the catheter with radius ψ.

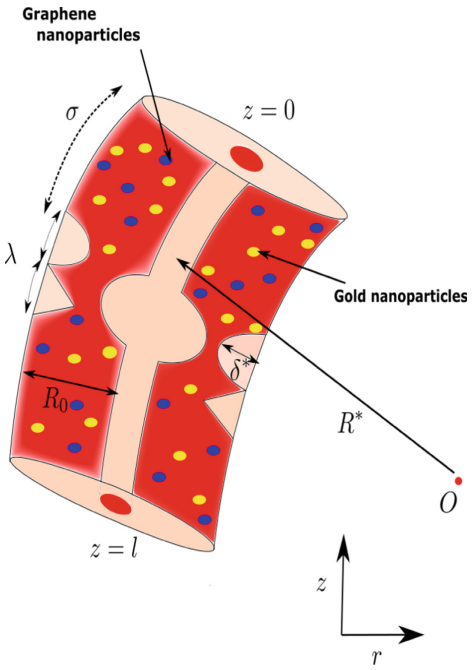

Fig. 1. Diseased artery segment

The mathematical representation of diseased segment [17]:
Stenosis:

$$\eta(z_1^*) = \begin{cases} R_0 - 2\frac{\delta}{\lambda}(z_1^* - d), & d \le z_1^* \le d + \frac{\lambda}{2} \\ R_0 + 2\frac{\delta}{\lambda}(z_1^* - d - \lambda), & d + \frac{\lambda}{2} \le z_1^* \le d + \lambda \\ R_0 + \frac{\delta}{\lambda} Sin(\pi(z_1^* - d)), & d + \lambda \le z_1^* \le d + 2\lambda \\ R_0 & \text{otherwise.} \end{cases} \tag{1}$$

Clot:

$$\epsilon(z_1^*) = \begin{cases} R_0(c + \sigma \exp(-\frac{\pi^2}{\lambda}(z_1^* - z_d^* - 0.5\lambda)^2)), & d < z_1^* < d + \frac{3\lambda}{2}, \\ cR_0, & \text{otherwise.} \end{cases} \tag{2}$$

where, σ is the maximum height of the clot at the axial position z_d^*, cR_0 is the radius of the inner tube with $c << 1$. In Eq. (1), δ represents the maximum height of the stenosis, d is the location of diseased segment.

Blood is assumed to be the suspension of red blood cells(RBCs), platelets, white blood cells, and plasma, etc. The migration of RBCs towards the center of the tube due to fluid shear resulted in the variation of viscosity and increase the fluid velocity towards the center resulting in more variation of RBCs distribution in the tube. To account for this variation of the blood viscosity due to spatial variation of RBCs, we proposed the hematocrit-dependent viscosity model:

$$\mu_f = \mu_0[1 + \gamma_1 h(r_1^*)], \tag{3}$$

where, $h(r_1^*) = h_m[1 - (\frac{r_1^*}{R_0})^m]$, h_m represent the maximum hematocrit at center with γ_1 as constant and $m \geq 2$ represent the exact shape of velocity profile.

2.1 Governing Equations

A uniform radial magnetic field B is applied on the diseased segment. The induced magnetic field is assumed to be negligible as it is very small as compared to the applied magnetic field. Subject to the above mention assumption with the MHD flow interaction, the resultant governing equations becomes [30]:

Continuity

$$\frac{\partial u_1^*}{\partial r_1^*} + \frac{u_1^*}{r_1^* + R^*} + \frac{R^*}{r_1^* + R^*}\frac{\partial w_1^*}{\partial z_1^*} = 0. \tag{4}$$

Momentum (in r_1^*-direction)

$$\rho_{hnf}\left[\frac{\partial u_1^*}{\partial t_1^*} + u_1^*\frac{\partial u_1^*}{\partial r_1^*} + \frac{w_1^* R^*}{r_1^* + R^*}\frac{\partial u_1^*}{\partial z_1^*} - \frac{{w_1^*}^2}{r_1^* + R^*}\right] = -\frac{\partial p}{\partial r_1^*} + \mu_{hnf}\left(\frac{\partial^2 u_1^*}{\partial {r_1^*}^2} + \frac{1}{r_1^* + R^*}\frac{\partial u_1^*}{\partial r_1^*}\right.$$
$$\left. + \left(\frac{R^*}{r_1^* + R^*}\right)^2\frac{\partial^2 u_1^*}{\partial z^2} - \frac{u_1^*}{(r_1^* + R^*)^2} - \frac{2R^*}{r_1^* + R^*}\frac{\partial w_1^*}{\partial z_1^*}\right) - \frac{\sigma_{hnf} B_0(-u_1^* + \beta_e w_1^*)}{(1 + \beta_e^2)}\left(\frac{R^*}{r_1^* + R^*}\right)^2$$
$$+ \left(\frac{4}{3}\frac{\partial u_1^*}{\partial r_1^*} - \frac{2}{3}\left(\frac{R^*}{R^* + r_1^*}\frac{\partial w_1^*}{\partial z_1^*} + \frac{u_1^*}{R^* + r_1^*}\right)\right)\frac{\partial \mu_{hnf}}{\partial r_1^*}. \tag{5}$$

Momentum (in z_1^*-direction)

$$\rho_{hnf}\left[\frac{\partial w_1^*}{\partial t_1^*}+u_1^*\frac{\partial w_1^*}{\partial r_1^*}+\frac{R^*}{r_1^*+R^*}\frac{\partial w_1^*}{\partial z_1^*}+\frac{u_1^* w_1^*}{r_1^*+R^*}\right]=-\left(\frac{R^*}{r_1^*+R^*}\right)\frac{\partial p}{\partial z_1^*}$$
$$+\mu_{hnf}\left(\frac{\partial^2 w_1^*}{\partial {r_1^*}^2}+\frac{1}{r_1^*+R^*}\frac{\partial w_1^*}{\partial r_1^*}+\left(\frac{R^*}{r_1^*+R^*}\right)^2\frac{\partial^2 w_1^*}{\partial {z_1^*}^2}-\frac{w_1^*}{(r_1^*+R^*)^2}+\frac{2R^*}{r_1^*+R^*}\frac{\partial u_1^*}{\partial z_1^*}\right)$$
$$+\left(\frac{R^*}{R^*+r_1^*}\frac{\partial u_1^*}{\partial z_1^*}+\frac{\partial w_1^*}{\partial r_1^*}-\frac{w_1^*}{R^*+r_1^*}\right)\frac{\partial \mu_{hnf}}{\partial r_1^*}+G(t_1^*)-\frac{\mu_{hnf}}{K}w_1^*$$
$$-\frac{\sigma_{hnf}B_0^2(\beta_e u_1^*+w_1^*)}{(1+\beta_e^2)}\left(\frac{R^*}{r_1^*+R^*}\right)^2. \tag{6}$$

where, the velocity (u,w) represent the velocity along the radial and axial direction respecively. The flow is independent in θ_1^* direction due to axi-symmetry blood flow in the artery. R^* represent the radius of curvature, t_1^* represent the time, β_e represent the Hall parameter, and K represent the permeability.

The associate dimensional boundary conditions are:

$$\begin{cases} w_1^*=0 & \text{at} \quad t_1^*=0, \\ w_1^*=0 & \text{at} \quad r_1^*=\eta(z_1^*) \quad \text{and} \quad r_1^*=\epsilon(z_1^*). \end{cases} \tag{7}$$

The arterial hemodynamic involves the analysis of pressure and waveform that are continuously changing due to the propogation of blood flow from central to peripheral arteries. The expression for axial pressure gradient is represented as [30]:

$$-\frac{\partial p}{\partial z_1^*}=A_0+A_1 cos(2\pi\omega_p t_1^*), t>0. \tag{8}$$

where, $\omega_p t_1^*=2\pi f_p$ with frequency f_p, A_0 and A_1 represents the mean and pulsatile component of pressure gradient, respectively. The extrinsic periodic body acceleration applied on the axial direction is given as [30]:

$$G(t_1^*)=B_0 cos(\omega_q t_1^*+\psi), \tag{9}$$

where, ψ is the phase angle, $\omega_q t_1^*=2\pi f_q$ with f_q as frequency and B_0 as the amplitude for body acceleration, respectively. Table 1 represents the thermophysical parameters for nanofluid and hybrid nanofluid.

2.2 Non-dimensionalization of Governing Equations

Apply the non-dimensional variables into Eqs. 1–2, one can obtain non-dimensionalize form of diseased artery:

Stenosis region:

$$\eta(z_1^*)=\begin{cases} 1-2\delta^*(z_1^*-d), & d\le z_1^*\le d+\frac{1}{2} \\ 1+2\delta^*(z_1^*-d-1), & d+\frac{1}{2}\le z_1^*\le d+1 \\ 1+\delta^* Sin(\pi(z_1^*-d)), & d+1\le z_1^*\le d+2 \\ 1 & \text{otherwise.} \end{cases} \tag{10}$$

Clot region:

$$\epsilon(z_1^*) = \begin{cases} c + \sigma \exp(-\pi^2(z_1^* - z_d^* - 0.5)^2), & d < z_1^* < d + 3/2, \\ c, & otherwise, \end{cases} \tag{11}$$

Table 1. Properties & Mathematical expression for nanofluid and hybrid nanofluid

Viscosity	$\mu_{nf} = \frac{\mu_f}{(1-\phi_1)^{2.5}}$ $\mu_{hnf} = \frac{\mu_{nf}}{(1-\phi_1)^{2.5}(1-\phi_2)^{2.5}}$
Density	$\rho_{nf} = (1-\phi_1)\rho_f + \phi_1\rho_{s_1}$ $\rho_{hnf} = [(1-\phi_2)\{(1-\phi_1)\rho_f + \phi_1\rho_{s_1}\}] + \phi_2\rho_{s_2}$
Electrical Conductivity	$\frac{\sigma_{nf}}{\sigma_f} = \frac{\sigma_{s_1}+(m-1)\sigma_f-(m-1)\phi_1(\sigma_f-\sigma_{s_1})}{\sigma_{s_1}+(m-1)\sigma_f+\phi_1(\sigma_f-\sigma_{s_1})}$ $\frac{\sigma_{hnf}}{\sigma_{nf}} = \frac{\sigma_{s_2}+(m-1)\sigma_f-(m-1)\phi_2(\sigma_f-\sigma_{s_2})}{\sigma_{s_2}+(m-1)\sigma_f+\phi_2(\sigma_f-\sigma_{s_2})}$

Table 2. Non-dimensional parameters

$\bar{r}_1^* = \frac{r_1^*}{R_0}$	$\bar{z}_1^* = \frac{z_1^*}{\lambda}$	$\bar{u}_1^* = \frac{\lambda u_1^*}{\delta^* U_0}$	$\bar{w}_1^* = \frac{w_1^*}{U_0}$
$\delta = \frac{\delta^*}{R_0}$	$\bar{t}_1^* = \frac{U_0 t_1^*}{R_0}$	$\bar{R}_c = \frac{R_c}{R_0}$	$\bar{p} = \frac{R_0^2 p}{\mu_0 U_0 \lambda}$
$Re = \frac{U_0\rho_f R_0}{\mu_f}$	$M^2 = \frac{\sigma_f B_0^2 R_0^2}{\mu_0}$	$Z = \frac{K}{R_0^2}$	$\beta_e = \omega_e \tau_e$

Again, use the non-dimensionalize parameters into Eqs. 4–6, neglecting the bar, and assuming the assumption of fully developed flow, mild stenosis ($\delta^* << 1$) with $O(1) = \alpha = \frac{R_0}{\lambda}$, the governing equations become:

$$\frac{dp}{dr_1^*} = 0, \tag{12}$$

$$\frac{\rho_{hnf}}{\rho_f} Re \frac{\partial w_1^*}{\partial t_1^*} = -\frac{R_c}{R_c + r_1^*}\frac{\partial p}{\partial z_1^*} + \frac{\mu_{hnf}}{\mu_0}\left(\frac{\partial^2 w_1^*}{\partial {r_1^*}^2} + \frac{1}{r_1^* + R_c}\frac{\partial w_1^*}{\partial r_1^*} - \frac{w_1^*}{(r_1^* + R_c)^2}\right) - \left(\frac{\partial w_1^*}{\partial r_1^*} + \frac{\partial w}{R_c + r_1^*}\right)\frac{m\beta_1 h_m {r_1^*}^{m-1}}{(1-\phi_1)^{2.5}(1-\phi_2)^{2.5}} + G(t_1^*) - \frac{\mu_{hnf}}{\mu_0}\frac{w_1^*}{Z} - \frac{\sigma_{hnf}}{\sigma_f}\left(\frac{R_c}{r_1^* + R_c}\right)^2 \left(\frac{1}{1+\beta_e^2}\right) M^2 w_1^*, \tag{13}$$

The associate boundary conditions are:

$$\begin{cases} w_1^* = 0 & \text{at} \quad t_1^* = 0, \\ w_1^* = 0, & \text{at} \quad r_1^* = \eta(z_1^*) \ \text{ and } \ r_1^* = \epsilon(z_1^*). \end{cases} \tag{14}$$

The non-dimensionalize formed for pressure gradient and body acceleration are given as follows:

$\frac{\partial p}{\partial z_1^*} = B_1(1 + e\cos c_1 t_1^*)$, $G(t_1^*) = B_2\cos(c_2 t_1^* + \chi)$, where $B_1 = \frac{A_0 R_0^2}{\mu_0 U_0}, e = \frac{A_1}{A_0}, B_2 = \frac{\bar{A}_0 R_0^2}{\mu_0 U_0}, c_2 = \frac{\bar{\omega}_2 R_0}{U_0}$.

In hemodynamic flow, the progression of arterial diseases can easily be understood by studying the basic hemodynamic factors like flow rate, impedance and wall shear stress. The mathematical expression for important hemodynamical factors such as wall shear stress, flow rate and resistive impedance are illustrated as [17,21]:

$$\tau_{w_1^*} = \left(\frac{\partial w_1^*}{\partial r_1^*}\right)_{r_1^* = \eta}, \tag{15}$$

$$Q = \int_{\epsilon}^{\eta} w_1^* r_1^* dr_1^*, \tag{16}$$

$$\lambda = \frac{L(\frac{\partial p}{\partial z_1^*})}{Q}. \tag{17}$$

3 Solution Process

The governing equations are highly non-linear and coupled, so a robust technique is used to solve these equations. To solve these equations, we employed the Crank-Nicholson method, which is unconditionally stable and second-order convergent in space and time. The partial and spatial derivatives are given as:

$$\frac{\partial w}{\partial r} = \frac{w_{i+1}^k - w_{i-1}^k}{2\Delta r}, \frac{\partial^2 w}{\partial^2 r} = \frac{w_{i+1}^k - 2w_i^k + w_{i-1}^k}{(\Delta x)^2}, \frac{\partial w}{\partial t} = \frac{w_i^{k+1} - w_i^k}{\Delta t}. \tag{18}$$

The flow chart of the schematic representation of the work plan is depicted in Fig. 2. The domain is divided into $N+1 \times M+1$ grid points, where N denotes the grid point in the spatial direction and M denotes the grid point in the time direction. The subscript i and j-designate for the nodal point in spatial and time direction, respectively. The value of w at initial time $t = 0$ is known due to the given condition. Every nodal point in the i^{th} level constitutes the tridiagonal system, which is solved using the Tri-diagonal Matrix Algorithm (TDMA). Thus, the value of w is known for each $(j+1)^{th}$ time level. Default values of parameters and thermodynamical properties of nanoparticles used in the present study are depicted in Table 3 and the Table 4 respectively.

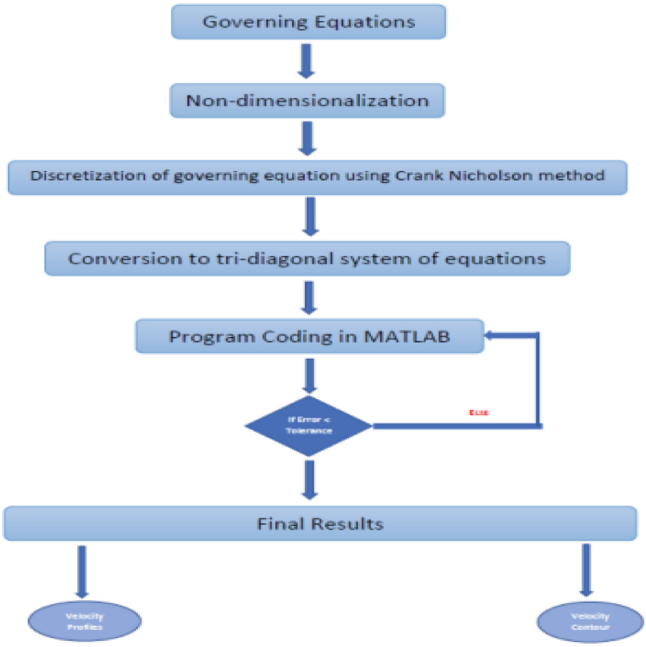

Fig. 2. Flow chart

Table 3. Dimensionless parameters

Parameter	ϕ_1	ϕ_2	δ	h_m	Re	M	R_c	β_e	e	B_1	B_2	Z
Value	0.02	0.02	0.1	1	2	1	3	0.5	0.2	0.25	5	3

Table 4. Thermophysical Properties

Thermophysical Properties	Blood	Gold	Graphene
Density $[\rho(Kg/m^3)]$	1063	19320	1800
Electrical Conductivity $[\sigma(S/m)]$	6.67×10^{-1}	4.52×10^{7}	6.3×10^{7}

4 Result and Discussion

The current study is validated using the published work of Elnaqeeb et al. [4], as shown in Fig. 3. To validate the result of present study with [4], we have reduced our model by considering striaght artery assumption $R_c = 0$. The Copper blood flow model is considered instead of (Au-GO). We ignore the multiple stenosis and used the stenosis model for $n = 2$ used by [4]. The velocity profile is drawn by assuming the same set of values as in [4]. There is a good agreement between velocity trend in our research work and trend of velocity profile in ref. [4]. In the present model, we have considered the curved artery as in more generalized cases,

the artery is not straight. Furthermore, we have included hematocrit dependent viscosity model on which very researchers published their work. It is one of the most essential parameter as its depict the picture of the spatial distribution of RBCs. The influence of hematocrit parameter on the velocity profile is depicted in the Fig. 4.

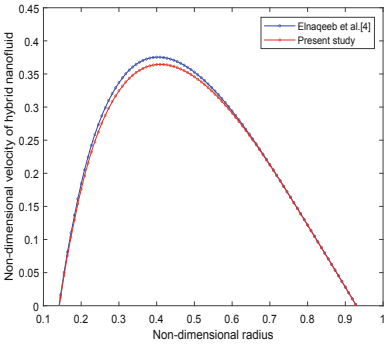

Fig. 3. Velocity profile for stensois shape parameter $n = 2$

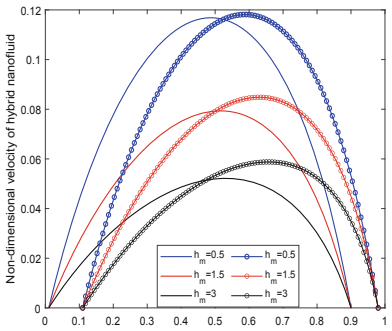

Fig. 4. Velocity profile for varying h_m

4.1 Velocity Profile

Blood undergoes a significant electromotive force when an external magnetic field is present. Haemoglobin contains magnetic iron ions, which significantly react to the surrounding magnetic field and affect blood flow. Red blood cells (RBCs) are magnetically repelled due to their inherent paramagnetic composition. From Fig. 4, we can inferred that the velocity profile decreases as the hematocrit parameter h_m enhances. The reduction in velocity profile is due to the increase in the blood viscosity. Figure 5 depicts the relationship between velocity profiles and magnetic field parameter M for clot and stenotic regions. The graph shows that the velocity profile in both cases will be higher in the absence of a magnetic field. As the value of the M increases from 0 to 4, the fluid velocity decreases as it experiences a resistive force known as Lorentz force. Figure 6 illustrates the effect of Hall parameter β_e on the velocity profile. The hall currents are induced due to the collision of the electrons under the action of a strong magnetic field that generates electromagnetic forces resulting in the modifying nature of the current density. It is observed from the figure that the velocity increases with an increase in the Hall parameter. This has happened because an upsurge in the Hall parameter signifies escalation in collision time or electron frequency, thus, assisting in the fluid velocity.

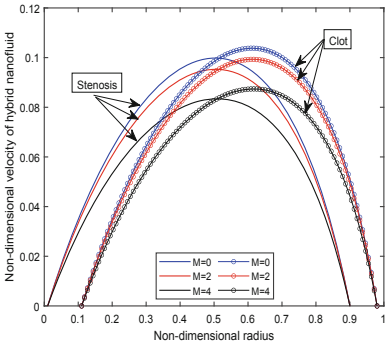

Fig. 5. Velocity profile for varying M

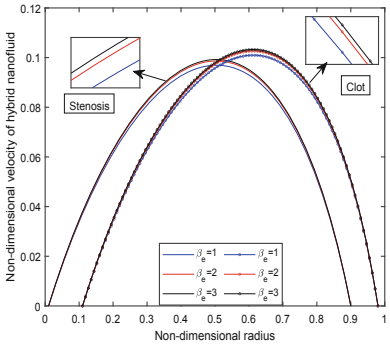

Fig. 6. Velocity profile for varying β_e

4.2 Flow Rate, Wall Shear Stress and Impedance

Figure 7 depicts the increment in flow rate with an upsurge in the radius of curvature parameter R_c. This increase may be explained by the fact that when the parameter Rc increases, the curved channel shrinks to a straight tube. The higher the value of R_c, the less obstruction comes in the fluid path, resulting in an upsurge in velocity profile with an increase in R_c. This study is helpful as its show that for smaller value of R_c, there is a significant growth in fear of deposition of plaque (lipid). A very less study has been conducted to show the radius of curvature effect, as in more generalised cases the artery is not always straight. Thus, it is essential to consider this effect into the model. It is noted from the Fig. 8 that the flow rate decreases as the magnetic field parameter M increases from 0 to 4. The non-dimensional velocity profile for M follows the same pattern as that of [28,29]. The flow rate is constant till $z = 2$; afterwards, the flow rate varies due to clot and stenosis, and it again attains its constant values after $z = 4$.

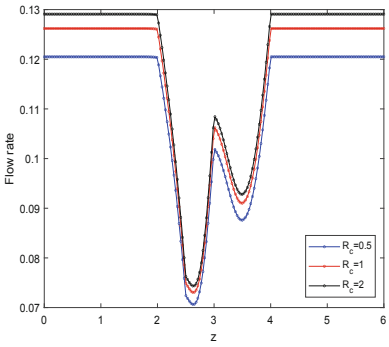

Fig. 7. Flow rate for varying R_c

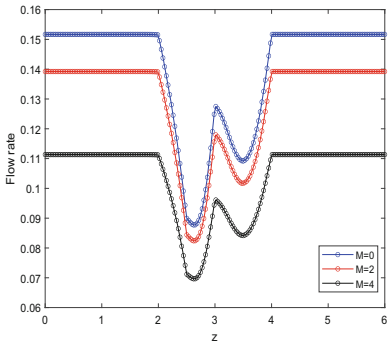

Fig. 8. Flow rate for varying M

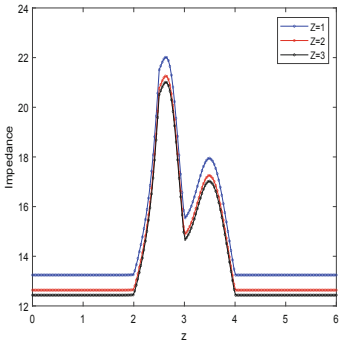

Fig. 9. Impedance for varying Z

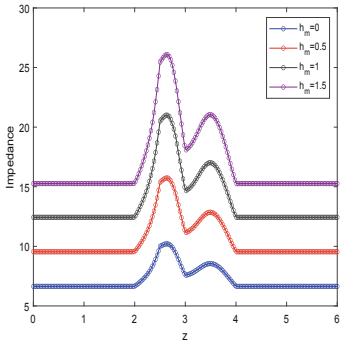

Fig. 10. Impedance for varying h_m

The existence of haemoglobin and magnetic iron oxide particles makes the blood to be profoundly impacted by a magnetic field. When a magnetic field is applied to an artery carrying blood, a strong electromotive field is generated known as the Lorentz force that results in the slowing down of the blood's flow. Thus, the fluid experiences the retarding force with an increment in parameter M, which resists the fluid flow, as observed in Fig. 8. The effect of the permeability parameter Z on the Impedance profile is demonstrated in Fig. 9. The ratio of the empty space to the total volume of the fluid medium is the porosity of the material [31]. Due to the dispersion of artery-clogging fatty cholesterol, blood clots, and plaques in the arterial lumen, blood is thought of as a porous medium. Increases in porosity result in more empty space, which in turn leads to less resistance to flow and increased blood velocity. As a result, the fluid velocity increases with the rise in the permeability parameter due to the less obstruction in its path. Thus, the impedance profile shows the declining nature as the permeability parameter Z increases. Figure 10 is plotted to see the variation of impedance profile with hematocrit dependent viscosity h_m. From these plots, it can be inferred that the impedance profile also increases with an increase in h_m. This has happened due to increases in fluid viscosity that resist the fluid motion and amplify the impedance profile. In arterial blood flow, the term "wall shear stress" refers to the force exerted per unit area on the fluid by the arterial wall (and vice versa) in a direction that is parallel to the local tangent plane. It is generally known that regions of arteries with either low or fluctuating wall shear stress seem more susceptible to atherosclerosis. The influence of the pressure gradient parameter B_1 on the WSS profile is seen in Fig. 11. The figure demonstrates the periodic nature and enhances with an increment in the B_1 parameter. The role of WSS with body acceleration parameter B_2 is depicted in Fig. 12. It is observed that the WSS profile varies periodically with time. As the magnitude of B_2 increases, the fluid velocity also increases, which leads to an enhancement in the amplitude of B_2.

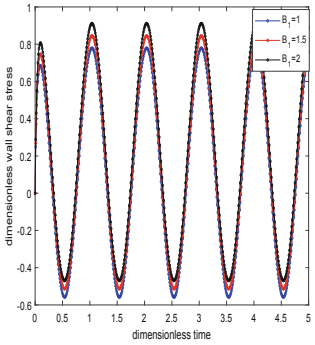

Fig. 11. Variation in WSS with varying B_1

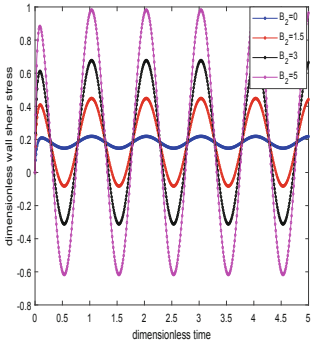

Fig. 12. Variation in WSS with varying B_2

4.3 Velocity Contour

Figure 13 illustrates the velocity contour for the varying height of stenosis and clot. It can be noted from the figure that the velocity decreases with an increase in the clot and stenosis height. There is a difference in the centre area that is occupied by the clot and the stenosis, despite the fact that the greatest velocity that can be achieved in each of the three scenarios being the same, which is 16×10^{-4}. As shown in the figure, the amplitude of the fluid velocity falls as the height of the clot and stenosis grows, which makes the flow of fluid more difficult to navigate.

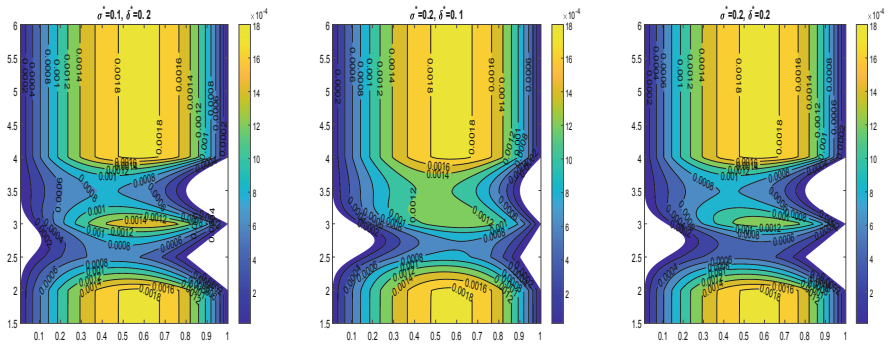

(a) (b) (c)

Fig. 13. Variation in blood flow patterns for diseased artery segment (a) $\sigma^* = 0.1, \delta^* = 0.2$, (b) $\sigma^* = 0.2, \delta^* = 0.1$ (c) $\sigma^* = 0.2, \delta^* = 0.2$.

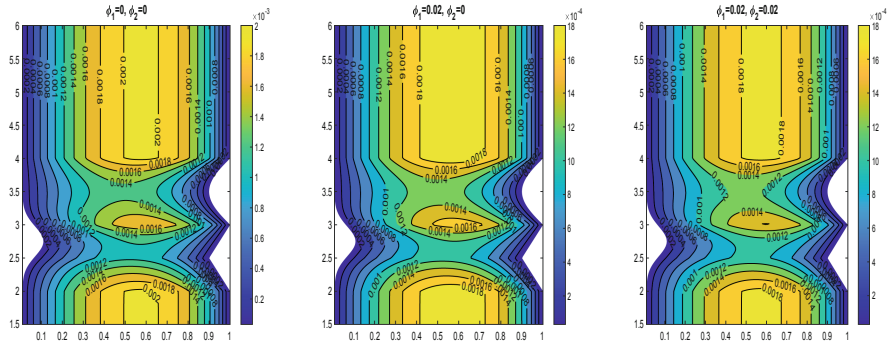

(a) (b) (c)

Fig. 14. Variation in blood flow patterns for different volume fractions of nanoparticles, (a) $\phi_1 = 0, \phi_2 = 0$, (b) $\phi_1 = 0.02, \phi_2 = 0$, (c) $\phi_1 = 0.02, \phi_2 = 0.02$.

Figure 14 highlights the effect of nanoparticles concentration ϕ_1 and ϕ_2 on the velocity contour. Figure 14a signifies the situation of pure blood when no nanoparticle is added. As we insert the gold nanoparticles into the blood, the fluid velocity decreases, as depicted in Fig. 14b. Further, the magnitude of the fluid velocity in the core area of the diseased artery is reduced as a result of the incorporation of graphene oxide with gold nanoparticles. Therefore, it could be beneficial for surgeons to manage the flow of blood.

5 Conclusion

A detailed study has been carried out to study the multiple stenotic arteries with thrombosis. The flow is subjected to the strong radial magnetic field, and the curvilinear coordinate is adapted to mimic the blood flow. There has been some thought given to the possibility of using a hybrid nanofluid created by suspending Au-GO nanoparticles in blood. Because of the extreme non-linearity of the governing equations, the robust implicit Crank-Nicholson method has been used. Starting with a discretization of the governing equations, a tridiagonal system is constructed for each nodal point on the $(i+1)^{th}$ level, and then the Tri-diagonal Matrix Algorithm (TDMA) is used to solve it. The velocity w at each mesh point may be calculated by using this method again for every $(j+1)^{th}$ time step. The effect of different pertinent parameters on velocity, temperature, wall shear stress, Impedance and velocity contour is displayed. The significant outcomes of the study are summarised below:

- The significant decline in flow velocity is observed for an increase in the stenosis and clot height.
- It has been observed that raising the Hall parameter induces an increase in fluid velocity owing to an increase in collision time or electron frequency, hence assisting fluid flow.

- Au-GO/blood hybrid nanoparticles have a higher velocity profile than pure blood and unitary nanoparticles.
- Increasing the permeability parameter Z allows the fluid to travel more freely, aiding the flow and decreasing the impedance profile.

The findings of this research may be useful in diagnostic imaging techniques for identifying vascular anomalies, such as magnetic resonance angiography (MRA). The hybrid nanoparticles Au-GO/blood have been studied due to their potential applicability in nanomedicine and biomedicine. Various stenosis forms (such as triangular and elliptical) and their tapering effects may be investigated in future studies, as can the interaction of nanoparticle shapes with permeable artery walls.

References

1. Prakash, O., Makinde, O.D., Singh, S.P., Jain, N., Kumar, D.: Effects of stenoses on non-Newtonian flow of blood in blood vessels. Int. J. Biomath. **8**(01), 1550010 (2015)
2. Doffin, J., Chagneau, F.: Oscillating flow between a clot model and a stenosis. J. Biomech. **14**(3), 143–148 (1981)
3. Strony, J., Beaudoin, A., Brands, D., Adelman, B.: Analysis of shear stress and hemodynamic factors in a model of coronary artery stenosis and thrombosis. Am. J. Physiol. Heart Circ. **265**(5), H1787–H1796 (1993)
4. Elnaqeeb, T., Mekheimer, K.S., Alghamdi, F.: Cu-blood flow model through a catheterized mild stenotic artery with a thrombosis. Math. Biosci. **282**, 135–146 (2016)
5. Sultan, F., Khan, N.A., Qasim, M., Afridi, M.I.: Numerical simulation of the flow of nano-Eyring-Powell fluid through a curved artery with time-variant stenosis and aneurysm. Nihon Reoroji Gakkaishi **47**(2), 75–85 (2019)
6. Akhtar, S., McCash, L.B., Nadeem, S., Saleem, A.: Scientific breakdown for physiological blood flow inside a tube with multi-thrombosis. Sci. Rep. **11**(1), 6718 (2021)
7. Mekheimer, K.S., El Kot, M.A.: Influence of magnetic field and Hall currents on blood flow through a stenotic artery. Appl. Math. Mech. **29**(8), 1093–1104 (2008)
8. Mishra, A., Sharma, B.K.: MHD mixed convection flow in a rotating channel in the presence of an inclined magnetic field with the Hall effect. J. Eng. Phys. Thermophys. **90**(6), 1488–1499 (2017)
9. Das, S., Barman, B., Jana, R.N., Makinde, O.D.: Hall and ion slip currents' impact on electromagnetic blood flow conveying hybrid nanoparticles through an endoscope with peristaltic waves. BioNanoScience **11**(3), 770–792 (2021)
10. Changdar, S., De, S.: Investigation of nanoparticle as a drug carrier suspended in a blood flowing through an inclined multiple stenosed artery. Bionanoscience **8**(1), 166–178 (2018)
11. Mekheimer, K.S., Hasona, W.M., Abo-Elkhair, R.E., Zaher, A.Z.: Peristaltic blood flow with gold nanoparticles as a third grade nanofluid in catheter: application of cancer therapy. Phys. Lett. A **382**(2–3), 85–93 (2018)
12. Kang, S., et al.: Gold nanoparticle/graphene oxide hybrid sheets attached on mesenchymal stem cells for effective photothermal cancer therapy. Chem. Mater. **29**(8), 3461–3476 (2017)

13. Liu, J., Dong, J., Zhang, T., Peng, Q.: Graphene-based nanomaterials and their potentials in advanced drug delivery and cancer therapy. J. Control. Release **286**, 64–73 (2018)
14. Khazayinejad, M., Hafezi, M., Dabir, B.: Peristaltic transport of biological graphene-blood nanofluid considering inclined magnetic field and thermal radiation in a porous media. Powder Technol. **384**, 452–465 (2021)
15. Sindhu, S., Gireesha, B.J., Sowmya, G., Makinde, O.D.: Hybrid nanoliquid flow through a microchannel with particle shape factor, slip and convective regime. Int. J. Numer. Methods Heat Fluid Flow **32**(10), 3388–3410 (2022)
16. Gandhi, R., Sharma, B.K., Kumawat, C., Bég, O.A.: Modeling and analysis of magnetic hybrid nanoparticle (au-al 2 o 3/blood) based drug delivery through a bell-shaped occluded artery with joule heating, viscous dissipation and variable viscosity effects. Proc. Inst. Mech. Eng. Part E: J. Process Mech. Eng. **236**(5), 2024–2043 (2022)
17. Sharma, B.K., Gandhi, R., Bhatti, M.M.: Entropy analysis of thermally radiating MHD slip flow of hybrid nanoparticles (Au-Al2O3/Blood) through a tapered multi-stenosed artery. Chem. Phys. Lett. **790**, 139348 (2022)
18. Singh, J., Rashidi, M.M., Kumar, D., et al.: A hybrid computational approach for Jeffery–Hamel flow in non-parallel walls. Neural Comput. Appl. **31**, 2407–2413 (2019). https://doi.org/10.1007/s00521-017-3198-y
19. Singh, J., Kumar, D., Baleanu, D., et al.: A hybrid analytical algorithm for thin film flow problem occurring in non-Newtonian fluid mechanics. Ain Shams Eng. J. **12**(2), 2297–2302 (2021)
20. Tripathi, B., Sharma, B.K.: Effect of variable viscosity on MHD inclined arterial blood flow with chemical reaction. Int. J. Appl. Mech. Eng. **23**(3), 767–785 (2018)
21. Kumawat, C., Sharma, B.K., Mekheimer, K.S.: Mathematical analysis of two-phase blood flow through a stenosed curved artery with hematocrit and temperature dependent viscosity. Phys. Scr. **96**(12), 125277 (2021)
22. Khanduri, U., Sharma, B.K.: Entropy analysis for MHD flow subject to temperature-dependent viscosity and thermal conductivity. In: Banerjee, S., Saha, A. (eds.) Nonlinear Dynamics and Applications. Springer Proceedings in Complexity, pp. 457–471. Springer, Cham (2022). https://doi.org/10.1007/978-3-030-99792-2_38
23. Prakash, J., Makinde, O.D.: Radiative heat transfer to blood flow through a stenotic artery in the presence of magnetic field. Lat. Am. Appl. Res. **41**(3), 273–277 (2011)
24. Sharma, B.K., Khanduri, U., Mishra, N.K., Chamkha, A.J.: Analysis of Arrhenius activation energy on magnetohydrodynamic gyrotactic microorganism flow through porous medium over an inclined stretching sheet with thermophoresis and Brownian motion. Proc. Inst. Mech. Eng. Part E: J. Process Mech. Eng. 09544089221128768 (2022)
25. Khanduri, U., Sharma, B.K.: Hall and ion slip effects on hybrid nanoparticles (Au-GO/blood) flow through a catheterized stenosed artery with thrombosis. Proc. Inst. Mech. Eng., Part C: J. Mech. Eng. Sci. 09544062221136710 (2022)
26. Sharma, B.K., Kumar, A., Gandhi, R., Bhatti, M.M.: Exponential space and thermal-dependent heat source effects on electro-magneto-hydrodynamic Jeffrey fluid flow over a vertical stretching surface. Int. J. Mod. Phys. B **36**(30), 2250220 (2022)
27. Gupta, S., Kumar, D., Singh, J.: Analytical study for MHD flow of Williamson nanofluid with the effects of variable thickness, nonlinear thermal radiation and

improved Fourier's and Fick's Laws. SN Appl. Sci. **2**(3), 1–12 (2020). https://doi.org/10.1007/s42452-020-1995-x
28. Tassaddiq, A., Khan, I., Nisar, K.S., Singh, J.: MHD flow of a generalized Casson fluid with Newtonian heating: a fractional model with Mittag-Leffler memory. Alex. Eng. J. **59**(5), 3049–3059 (2020)
29. Sheikh, N.A., Ching, D.L.C., Khan, I., Kumar, D., Nisar, K.S.: A new model of fractional Casson fluid based on generalized Fick's and Fourier's laws together with heat and mass transfer. Alex. Eng. J. **59**(5), 2865–2876 (2020)
30. Sharma, B.K., Kumawat, C., Vafai, K.: Computational biomedical simulations of hybrid nanoparticles (Au-Al2O3/blood-mediated) transport in a stenosed and aneurysmal curved artery with heat and mass transfer: Hematocrit dependent viscosity approach. Chem. Phys. Lett. **800**, 139666 (2022)
31. Sharma, B.K., Khanduri, U., Mishra, N.K., Mekheimer, K.S.: Combined effect of thermophoresis and Brownian motion on MHD mixed convective flow over an inclined stretching surface with radiation and chemical reaction. Int. J. Mod. Phys. B 2350095 (2022)